

PriorMapNet: Enhancing Online Vectorized HD Map Construction with Priors

Rongxuan Wang^{1†} Xin Lu² Xiaoyang Liu² Xiaoyi Zou² Tongyi Cao² Ying Li^{*1}

¹Beijing Institute of Technology
rongxuan_wang@foxmail.com

²DeepRoute.ai
ying.li@bit.edu.cn

Abstract

Online vectorized High-Definition (HD) map construction is crucial for subsequent prediction and planning tasks in autonomous driving. Following MapTR paradigm, recent works have made noteworthy achievements. However, reference points are randomly initialized in mainstream methods, leading to unstable matching between predictions and ground truth. To address this issue, we introduce PriorMapNet to enhance online vectorized HD map construction with priors. We propose the PPS-Decoder, which provides reference points with position and structure priors. Fitted from the map elements in the dataset, prior reference points lower the learning difficulty and achieve stable matching. Furthermore, we propose the PF-Encoder to enhance the image-to-BEV transformation with BEV feature priors. Besides, we propose the DMD cross-attention, which decouples cross-attention along multi-scale and multi-sample respectively to improve efficiency. Our proposed PriorMapNet achieves state-of-the-art performance in the online vectorized HD map construction task on nuScenes and Argoverse2 datasets. The code will be released publicly soon.

1 Introduction

High-Definition (HD) map is integral to autonomous driving, offering detailed information on critical elements such as road boundaries, traffic lanes, and pedestrian crossings (Li et al. 2022b; Liao et al. 2022). This detailed information is crucial for subsequent tasks like trajectory forecasting (Liang et al. 2020; Zhou et al. 2022) and path planning (Hu et al. 2023). Traditionally, HD map has been constructed using offline SLAM-based methods, which are time-consuming and do not scale effectively with the rapid updates of urban environments and road networks. To address these challenges, there is growing interest in online HD map construction methods that use vehicle-mounted sensors to generate maps in real-time. Early approaches (Li et al. 2022d; Peng et al. 2023) focus on semantic segmentation in bird’s eye view (BEV). However, these methods primarily predict rasterized maps, which lack the vectorized map information for autonomous driving tasks.

Following DETR (Carion et al. 2020) paradigm, recent advancements have introduced end-to-end learning frameworks aimed at directly predicting vectorized instances.

[†] Work done during the internship at DeepRoute.ai.

^{*} Corresponding author.

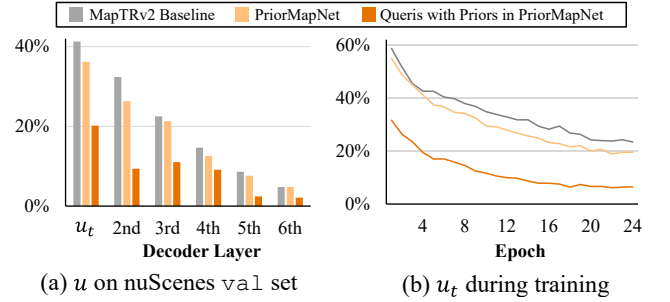


Figure 1: Comparison of the unstable matching scores, the lower, the better. (a) and (b) denote the unstable matching scores during validation and training, respectively. u means the percentage of queries whose GT match changed compared with the previous decoder layer, and u_t means the percentage of final output queries whose GT match changed compared with the first decoder layer. “Queris with Priors” denote the queries corresponding to Prior Reference Points.

MapTR (Liao et al. 2022) and MapTRv2 (Liao et al. 2023) design an instance-point level hierarchical query embedding scheme and have demonstrated promising outcomes in constructing vectorized HD maps. The mainstream methods proposed later follow this pipeline, with improvements focusing on enhancing interactions between queries and integrating external features (Xu, Wong, and Zhao 2023; Liu et al. 2024a; Zhou et al. 2024).

In these methods, queries learn the position and structure of map elements and are matched with the ground truth (GT) during training. However, the Hungarian algorithm used for matching is sensitive to small changes in the cost matrix, which leads to *unstable matching* (Li et al. 2022a). To quantify the instability of matching, we define the unstable matching score u following Stable-DINO (Liu et al. 2023a), representing the percentage of queries whose GT match changed compared with the previous decoder layer. We also measure the total unstable matching score u_t , which represents the percentage of final output queries whose GT match changed compared with the first decoder layer. As shown in Fig. 1, MapTRv2 exhibits unstable matching throughout the process of training and validation.

Why the matching is unstable? The training process

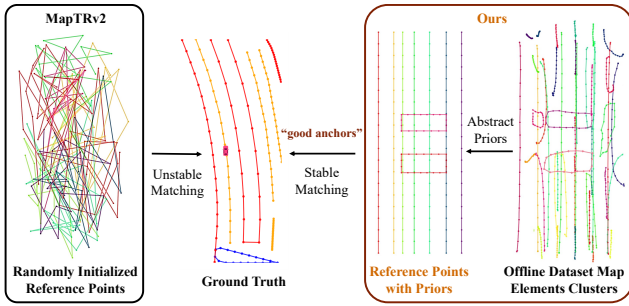


Figure 2: Comparison of the matching of MapTRv2 and our proposed method. Reference points with position and structure priors achieve stable matching.

of DETR-like models has two stages: learning “good anchors” (stage I) and learning relative offsets (stage II) (Li et al. 2022a). In mainstream methods, queries consist of content embeddings and position embeddings. Position embeddings generate reference points for sampling (related to stage I), and content embeddings generate sampling offsets and attention weights (related to stage II). Position embeddings are learnable and initialized randomly, which leads to reference points that are distributed without any specific structure. In contrast, the vectorized HD map consists of map elements like polylines or polygons connected in an ordered sequence, with distinct positional distributions and geometric patterns. As shown in Fig. 2, matching these structured map elements with randomly distributed reference points is challenging and results in unstable matching. To solve this problem, we propose the Decoder with Prior Position and Structure (PPS-Decoder). By fitting the distribution of map elements in datasets through clustering and abstracting these distributions as priors, the reference points are enhanced to better match the positional and structural features of map elements. As demonstrated in Tab. 4, prior-aware queries improve both accuracy and matching stability by reducing the difficulty of learning “good anchor”.

In essence, the prior is an effective initialization method, reducing the learning difficulty for the model. To leverage this approach, we introduce the Encoder with Prior Feature (PF-Encoder). PF-Encoder transforms image features into initialized BEV features, which are utilized as BEV query priors and optimized in the encoder. Discriminative Loss is introduced to better aggregate map elements embeddings. Besides, BEV features are downsampled to multi-scale, bringing computational complexity. To enhance efficiency, we propose the Decoupled Multi-Scale Deformable Cross-Attention (DMD cross-attention), which decouples cross-attention along multi-scale and multi-sample respectively. The combination of the PF-Encoder, PPS-Decoder, and DMD cross-attention forms our proposed PriorMapNet.

Extensive experiments are conducted to prove our superiority. We achieve state-of-the-art (SOTA) performance in online vectorized HD map construction on nuScenes (Caesar et al. 2020) and Argoverse2 (Wilson et al. 2023) datasets. Furthermore, experiments conducted under various settings demonstrate the robustness and generalization capabilities

of PriorMapNet. In summary, our contributions are:

- We introduce a novel prior-based framework for online HD map construction by integrating feature, position, and structure priors into encoder and decoder.
- We propose the DMD cross-attention, which decouples cross-attention along multi-scale and multi-sample respectively to improve efficiency.
- We achieve SOTA performance in online vectorized HD map construction on the nuScenes and Argoverse2 datasets, demonstrating both high performance and generalization capability.

2 Related Work

2.1 Online Vectorized HD Map Construction

Unlike traditional offline HD map construction methods, recent studies use vehicle-mounted sensors to construct online HD map. Early methods (Phillion and Fidler 2020; Li et al. 2022d; Liu et al. 2022b) tackle map construction as a segmentation task, predicting rasterized maps in BEV space. HDMapNet (Li et al. 2022b) further converts these rasterized maps into vectorized maps through post-processing.

VectorMapNet (Liu et al. 2023b) introduces the first end-to-end vectorized map model, using a DETR (Carion et al. 2020) decoder to detect map elements and optimizing results with an auto-regressive transformer. Subsequently, MapTR (Liao et al. 2022) and MapTRv2 (Liao et al. 2023) design a one-stage map construction paradigm with an instance-point level hierarchical query embedding scheme. The mainstream methods proposed later follow this pipeline, with improvements focusing on enhancing interactions of queries and external features. InsMapper (Xu, Wong, and Zhao 2023) and HIMap (Zhou et al. 2024) further explore the correlation between instances and points and improve the interaction within queries. MapQR (Liu et al. 2024b) implicitly encodes point-level queries within instance-level queries and embeds query positions like Conditional DETR (Meng et al. 2021). Despite the above developments, these methods randomly initialize reference points, resulting in unstable matching. To address this issue, our PriorMapNet introduces priors to enhance matching stability.

2.2 Priors for HD Map Construction

Priors provide effective initialization for map construction and reduce the difficulty of model learning. We categorize priors into two types: semantic priors and positional and structural priors. For prior semantics, MGMap (Liu et al. 2024a) proposes Mask-Active Instance (MAI), which learns map instance segmentation results and provides semantic priors for instance queries. Bi-Mapper (Li et al. 2023a) designs a two-stream model, using priors from global and local perspectives to enhance semantic map learning. For prior position and structure, Topo2D (Li et al. 2024a) uses 2D lane detection results as priors to initialize queries. SMERF (Luo et al. 2023) and P-MapNet (Jiang et al. 2024) introduce Standard Map (SDMap) as position and structure priors for map construction. However, the above methods rely on additional modules, increasing computational complexity. In contrast,

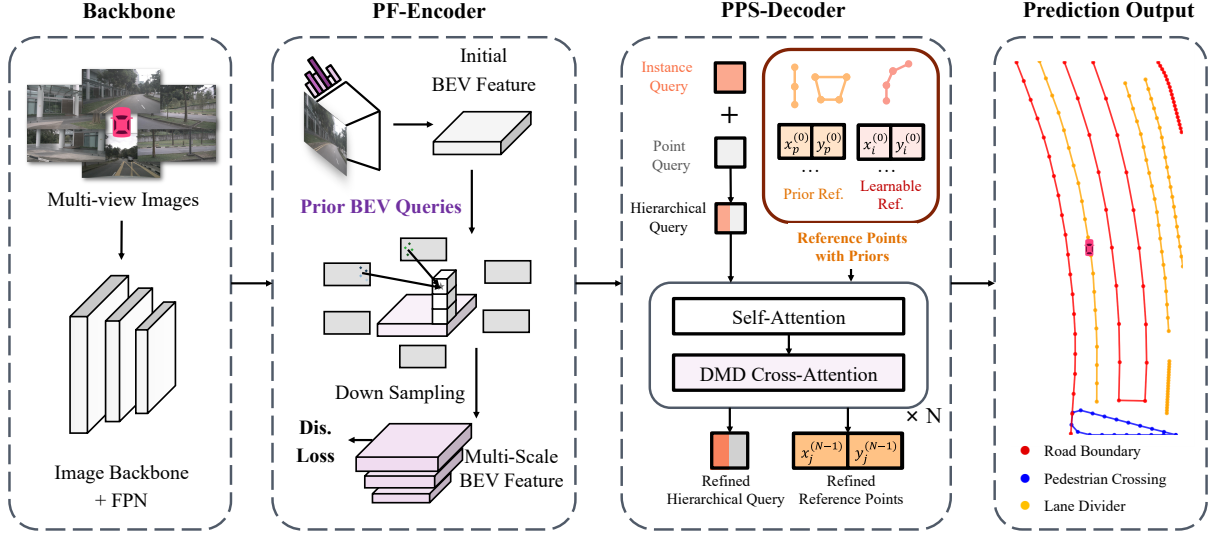


Figure 3: The overview of our proposed PriorMapNet. Given multi-view images as input, the output is a set of map elements. PriorMapNet consists of three modules: the backbone, the PF-Encoder and the PPS-Decoder. The backbone extracts image features by using the ResNet and a FPN neck. The PF-Encoder transforms image features into BEV and downsamples it to multiple scales. The PPS-Decoder predicts map elements through Transformer, and reference points with priors are used for stable matching. In the cross-attention layer, the DMD cross-attention is used to achieve efficiency.

PriorMapNet uses offline clustered map elements as position and structure priors, improving performance without additional computational consumption.

2.3 Image-to-BEV Encoder for Map Construction

Map construction usually relies on the BEV feature, which is transformed from images by the encoder. There are two types of encoders: bottom-up and top-down. Bottom-up encoders (Phillion and Fidler 2020; Huang et al. 2021; Li et al. 2022c, 2023b) lift images to 3D and use voxel pooling to generate BEV features. Top-down encoders (Wang et al. 2022; Li et al. 2022d; Yang et al. 2023; Chen et al. 2022) generate BEV queries containing 3D information and extract image features to BEV queries with the transformer. However, since queries are randomly initialized, the single-layer encoder results in low accuracy (Liao et al. 2022), and the multi-layer encoder brings more computational complexity (Liu et al. 2024b; Li et al. 2024b). To overcome these limitations, we enhance BEV queries with prior features.

3 Method

3.1 Overview

Fig. 3 shows the overall pipeline of our method. Given N_c multi-view images $\{I_i\}_{i=1}^{N_c}$ as input, the output is a set of N_m map elements $\{M_i\}_{i=1}^{N_m}$. Each map element is defined as a class label c and an ordered point sequence $\{(x_i, y_i)\}_{i=1}^{N_p}$, where N_p is the number of points in each map element.

Based on MapTRv2 (Liao et al. 2023), our method consists of three modules: the backbone, the PF-Encoder and the PPS-Decoder. The backbone extracts multi-scale image features $\{F_{img}^i\}_{i=1}^{N_c}$ by ResNet (He et al. 2016) and

a FPN (Lin et al. 2017) neck. The PF-Encoder transforms images features to BEV features $F_{BEV} \in \mathbb{R}^{H \times W \times C}$ and downsamples it to multiple scales, as described in Section 3.3. The PPS-Decoder predicts map elements through transformer, and reference points with priors are used for stable matching, as detailed in Section 3.2. In the cross-attention layer, we introduce the DMD cross-attention to achieve efficiency, as described in Section 3.4. We start by detailing the PPS-Decoder, which is the core of our method.

3.2 Decoder with Prior Position and Structure

The pipeline of our PPS-Decoder is shown in Fig. 4c. Compared with MapTRv2, which randomly initializes reference points, and MGMap, which only provides semantic priors without position information, the PPS-Decoder enhances reference points with position and structure priors, providing “good anchor” to improve accuracy and matching stability.

The PPS-Decoder contains several cascaded decoder layers to refine the hierarchical queries and reference points iteratively. Hierarchical queries consist of instance-level queries $q_{ins} \in \mathbb{R}^{N_I \times C}$ and point-level queries $q_{pts} \in \mathbb{R}^{N_P \times C}$, which are combined through broadcasting:

$$q = q_{ins} + q_{pts}, q \in \mathbb{R}^{N_I \times N_P \times C}. \quad (1)$$

Reference points are initialized with prior position and structure. To fit the distribution of map elements in the dataset, we use K-Means to cluster map elements and abstract the position information of the first N_{pri} elements, as shown in Fig. 2. Clustering and abstraction are done offline, ensuring no additional computational burden during inference. During training and inference, some reference points obtain the fitted position and structure priors (called

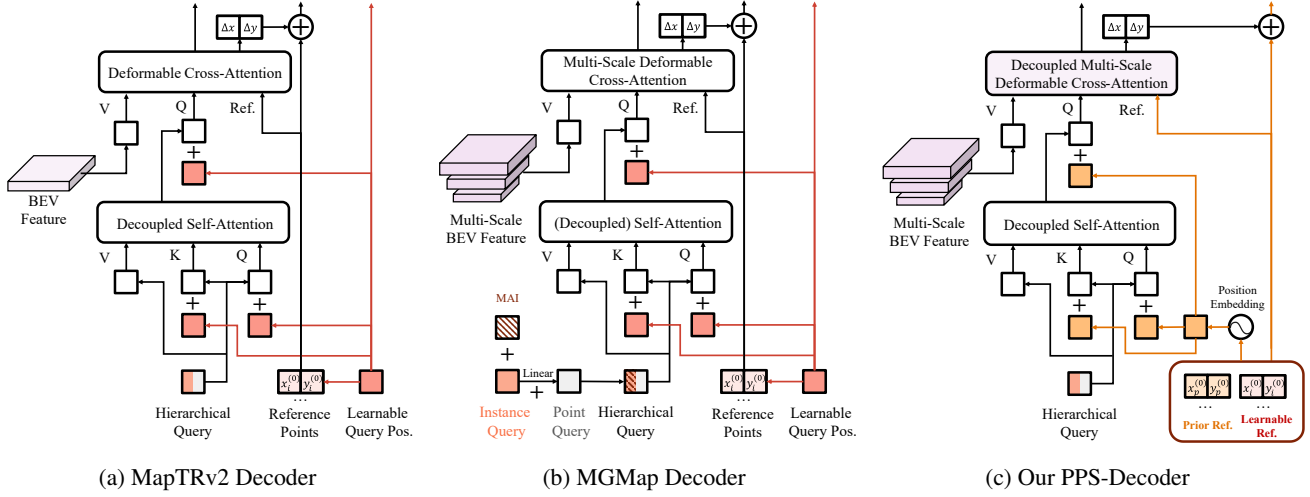


Figure 4: Comparison of the decoder of MapTRv2, MGMap and our proposed PriorMapNet. For simplicity, we only show the first layer in the transformer decoder. (a) MapTRv2 uses randomly initialized learnable query positions for all layers without any adaptation, which brings unstable matching results. (b) MGMap adds Mask-Activated Instance to provide semantic priors, but lacks position information. In contrast, (c) PriorMapNet enhances reference points with priors, which achieves stable matching.

Prior Reference Points, $R_{\text{pri}} \in \mathbb{R}^{N_{\text{pri}} \times N_P \times 2}$), while the rest of the reference points are still from learnable parameters (called Learnable Reference Points, $R_{\text{lrn}} \in \mathbb{R}^{N_{\text{lrn}} \times N_P \times 2}$). The combined set of reference points is denoted as $R = \{R_{\text{pri}}, R_{\text{lrn}}\}$, where the total number of instance queries is $N_I = N_{\text{pri}} + N_{\text{lrn}}$.

To embed query position, reference points are encoded with sinusoidal positions following DAB-DETR (Liu et al. 2022a). Query position embedding is achieved as follows:

$$q_{\text{pos}} = \text{Linear}(\text{PE}(R)), \mathbb{R}^{N_I \times N_P \times 2} \rightarrow \mathbb{R}^{N_I \times N_P \times C}, \quad (2)$$

where $\text{PE}(\cdot)$ generates sinusoidal embeddings based on reference points coordinates (Vaswani et al. 2017). The parameters of linear layers are not shared across decoder layers. $\text{PE}(\cdot)$ is calculated separately on coordinates, and position embeddings are concatenated along feature channels:

$$\text{PE}(R) = \text{PE}(x_r, y_r) = \text{Cat}(\text{PE}(x_r), \text{PE}(y_r)). \quad (3)$$

Reference points and position embeddings are updated across the PPS-Decoder layers. In each layer, self-attention and cross-attention mechanisms use the following inputs for queries, keys, values, and reference points:

$$\begin{cases} \text{Self-Attn} : Q = q + q_{\text{pos}}, K = q + q_{\text{pos}}, V = q, \\ \text{Cross-Attn} : Q = q + q_{\text{pos}}, V = F_{\text{BEV}}, R = R. \end{cases} \quad (4)$$

The Prior Reference Points fit the position and structure distribution of the map elements in the dataset, which helps queries concentrate on learning the offsets from reference points. In addition, we maintain Learnable Reference Points to capture and represent map elements that deviate from typical position and structure patterns. The self-attention enables interaction between Prior Reference Points and Learnable Reference Points, reducing redundant detections and improving overall detection accuracy.

3.3 Encoder with Prior Feature

PF-Encoder enhances the image-to-BEV transformation with BEV feature priors. Built on the foundation of top-down encoders, such as BEVFormer (Li et al. 2022d) and GKT (Chen et al. 2022), PF-Encoder leverage BEV features as queries to extract relevant image features via cross-attentions.

We first utilize LSS (Phillion and Fidler 2020) to transform image features into initialized BEV features, which are then used as BEV query priors, optimized in a single-layer BEVFormer (Li et al. 2022d) encoder. Following MGMap (Liu et al. 2024a), BEV features are downsampled to multi-scale with an EML neck.

For queries to better aggregate features from the same map element, it is necessary to assimilate the embeddings of the same instance and distinguish the embeddings of different instances. Therefore, we introduce Discriminative Loss of map elements (Neven et al. 2018) to bring the same instance closer and separate different instances further:

$$\begin{cases} L_{\text{var}} = \frac{1}{K} \sum_{k=1}^K \frac{1}{p_n} \sum_{l=1}^{p_n} [\|\mu_k - e_l\| - \delta_v]_+^2, \\ L_{\text{dist}} = \frac{1}{K(K-1)} \sum_{i=1}^K \sum_{j=1, i \neq j}^K [\delta_d - \|\mu_i - \mu_j\|]_+^2, \end{cases} \quad (5)$$

where L_{var} pulls the embeddings e_i of K map elements toward their respective means μ_n , and L_{dist} pushes away the mean embeddings of different map elements. p_n represents the number of grids of map elements. $\|\cdot\|$ is the L2 distance and $[x]_+ = \max(0, x)$. δ_v and δ_d are the borders of the variance and distance loss. The total Discriminative Loss is defined as $L_{\text{dis}} = \lambda_1 L_{\text{var}} + \lambda_2 L_{\text{dist}}$.

In the cross-attention layer of the PPS-Decoder, queries weighted sample BEV features. PF-Encoder enables the queries to effectively aggregate features associated with the

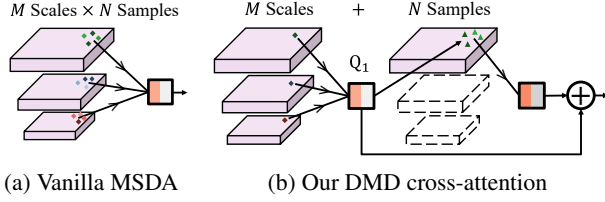


Figure 5: Comparison of the vanilla MSDA and our proposed DMD cross-attention. DMD cross-attention performs cross-attention along multi-scale and multi-sample respectively to achieve efficiency.

same map element while distinguishing between different map instances, improving the accuracy of map construction.

3.4 Decoupled Multi-Scale Deformable Attention

To address the computational complexity of multi-scale deformable cross-attention (MSDA), we propose the DMD cross-attention mechanism to decouple cross-attention along multi-scale and multi-sample, as shown in Fig. 5b.

In vanilla MSDA (Zhu et al. 2020), each query interacts with M -scale BEV features and N points are sampled at each scale, whose computation complexity is $O(M \times N)$:

$$\text{MSDA}(Q, V, R) = \sum_{i=1}^{N_h} W_i \sum_{j=1}^M \sum_{k=1}^N A_{ijk} \cdot W'_i V_j (R + O_{ijk}), \quad (6)$$

where N_h is the number of attention heads. $A_{ijk} \in [0, 1]$ and $O_{ijk} \in \mathbb{R}^2$ are attention weight and sampling offset respectively, which are generated from Q . $A_{ijk} \in [0, 1]$ is normalized by $\sum_{j=1}^M \sum_{k=1}^N A_{ijk} = 1$. $W_i \in \mathbb{R}^{C \times (C/N_h)}$ and $W'_i \in \mathbb{R}^{(C/N_h) \times C}$ are learnable weights.

To improve efficiency, the DMD cross-attention mechanism decouples the vanilla MSDA process into two stages:

$$\begin{cases} Q_1 = \text{Linear}_1(\text{MSDA}_1(Q, V, R)), \\ Q_{\text{output}} = Q_1 + \text{Linear}_2(\text{MSDA}_2(Q_1, V_1, R)), \end{cases} \quad (7)$$

where $\text{MSDA}_1(\cdot)$ and $\text{MSDA}_2(\cdot)$ denote $\text{MSDA}(\cdot)$ at $N = 1$ and $M = 1$ respectively. V_1 is the largest scale BEV feature. The multi-scale stage performs cross-attention across M scales and samples one point per scale. The multi-sample stage uses the output from the multi-scale stage and focuses on the largest scale feature to sample N points. DMD cross-attention reduces the computation complexity to $O(M + N)$ and achieves higher performance than vanilla MSDA.

4 Experiments

4.1 Datasets and Metrics

To validate the effectiveness of our proposed method PriorMapNet, we evaluate it on the widely used nuScenes dataset (Caesar et al. 2020) and Argoverse 2 dataset (Wilson et al. 2023) and compare it with the SOTA methods.

The nuScenes dataset is a standard benchmark for online vectorized HD map construction, featuring 1000 driving scenes captured by six multi-view cameras and LiDAR,

with 2D vectorized map elements as ground truth. Argoverse 2 is designed for perception and prediction studies in autonomous driving, containing 1000 scenes of 15 seconds each. 3D vectorized map elements captured by seven multi-view cameras are provided as ground truth.

Following the previous studies (Li et al. 2022b; Liao et al. 2022), we evaluate performance across three categories of map elements: lane dividers, pedestrian crossings, and road boundaries. The performance of PriorMapNet is assessed using the Average Precision (AP) metric, where a prediction is considered a True Positive if the Chamfer Distance between the prediction and its ground truth is within thresholds of 0.5, 1.0, and 1.5 meters.

4.2 Implementation Details

Our model is trained on 8 NVIDIA A100 GPUs with a batch size of 8×3 . Unless otherwise specified, the number of training epochs is 24 on nuScenes and 6 on Argoverse 2. The BEV range is $[-30\text{m}, 30\text{m}]$ along the longitudinal axis and $[-15\text{m}, 15\text{m}]$ along the lateral axis, with a feature size $H \times W$ of 200×100 . The number of instance queries N_I , prior queries N_{pri} and point queries N_P are set to 50, 9 and 20, respectively. Both λ_1 and λ_2 are set to 1. δ_v is 0.5 and δ_d is 3. Other settings keep in line with MapTRv2. The supplementary material shows more implementation details and ablation studies on hyperparameters.

4.3 Main Results

Results on nuScenes. We report quantitative results on nuScenes val set in Tab. 1. Under camera modality, PriorMapNet surpasses previous SOTA methods and achieves 6.2% mAP improvement compared with our baseline MapTRv2. On one RTX 4090 GPU, PriorMapNet infers at 13.9 frames per second (FPS). Additionally, under the camera and lidar fusion modality, PriorMapNet reaches 72.9% mAP and 7.5 FPS, demonstrating strong generalization capabilities. Qualitative results are shown in Fig. 6, further illustrating that PriorMapNet achieves improved results. More qualitative results are shown in the supplementary material.

Results on Argoverse 2. We report quantitative results on Argoverse 2 val set in Tab. 2. Argoverse 2 provides 3D map annotations, allowing predictions for both 2D and 3D map elements. PriorMapNet surpasses previous SOTA methods in both dimensions, achieving 72.0% mAP for 2D map elements and 69.9% mAP for 3D map elements with an inference speed of 12.6 FPS. Experimental results demonstrate the generalizability of our method.

Results on Enlarged BEV Range. We train and evaluate models on enlarged BEV ranges on nuScenes val set as shown in Tab. 3. The size of the BEV grid is maintained at $[0.3\text{m}, 0.3\text{m}]$. To verify the robustness of our method, we correspondingly enlarge the prior clustering and position range of map elements. Other settings remain in line with the original models. Experimental results demonstrate that PriorMapNet maintains superiority on enlarged BEV ranges. Notably, under the range of $100 \times 50\text{m}$, our method outperforms the SOTA method SQD-MapNet (Wang et al. 2024) which integrates stream strategy.

Method	Modality	Backbone	Epoch	AP _{div}	AP _{ped}	AP _{bou}	mAP	FPS
MapTRv2 [arxiv23]	C	R50	24	60.5	60.5	61.8	60.9	16.7
MGMap* [CVPR24]	C	R50	24	65.0	61.8	67.5	64.8	-
HIMap [CVPR24]	C	R50	30	68.4	62.6	69.1	66.7	-
InsMapper [ECCV24]	C	R50	24	65.1	61.6	64.6	63.8	-
MapQR [ECCV24]	C	R50	24	68.7	63.4	67.7	66.4	16.2
PriorMapNet (Ours)	C	R50	24	69.0	64.0	68.2	67.1	13.9
MapTRv2 [arxiv23]	C	R50	110	68.3	68.1	69.7	68.7	16.7
MGMap [CVPR24]	C	R50	110	64.4	67.6	67.7	66.5	18.0
MapQR [ECCV24]	C	R50	110	74.4	70.1	73.2	72.6	16.2
PriorMapNet (Ours)	C	R50	110	73.2	71.5	73.3	72.7	13.9
HDMaNet [ICRA22]	C & L	EB0 & PP	30	29.6	16.3	46.7	31.0	0.6
MapTRv2 [arxiv23]	C & L	R50 & Sec	24	66.5	65.6	74.8	69.0	7.8
MGMap [CVPR24]	C & L	R50 & Sec	24	71.1	67.7	76.2	71.7	7.5
PriorMapNet (Ours)	C & L	R50 & Sec	24	72.4	70.1	76.2	72.9	7.5

Table 1: Quantitative evaluation on nuScenes val set. “C” and “L” respectively refer to multi-view cameras and LiDAR inputs. “R50”, “EB0”, “PP” and “Sec” denote ResNet50 (He et al. 2016), EfficientNet-B0 (Tan and Le 2019), PointPillars (Lang et al. 2019) and SECOND (Yan, Mao, and Li 2018) respectively. “MGMap*” means MGMap based on MapTRv2. FPS is tested on a single RTX 4090 GPU for fair comparison. “-” means the corresponding results are not available.

Dim.	Method	AP _{div}	AP _{ped}	AP _{bou}	mAP	FPS
2	MapTRv2	71.5	63.6	67.4	67.5	15.2
	HIMap	69.5	69.0	70.3	69.6	-
	MapQR	72.3	64.3	68.1	68.2	14.2
	PriorMapNet	75.4	69.3	71.3	72.0	12.6
3	MapTRv2	68.9	60.7	64.5	64.7	15.0
	HIMap	68.3	66.7	70.3	68.4	-
	MapQR	71.2	60.1	66.2	65.9	14.1
	PriorMapNet	73.4	66.5	69.8	69.9	12.6

Table 2: Quantitative evaluation on Argoverse 2 val set. PriorMapNet reaches SOTA performance, validating its generalization ability. Since Argoverse 2 provides 3D map annotation, “Dim.” represents the dimension used to model map elements. When the map dimension is 2, the height information of map elements is dropped, and when the map dimension is 3, the 3D map elements are predicted directly. FPS is tested on a single RTX 4090 GPU for fair comparison. “-” means the corresponding results are not available.

4.4 Ablation Study

We conduct ablation experiments on nuScenes to verify the effectiveness of our proposed modules and their designs. All models are trained for 24 epochs, and the BEV range is 60×30m. As shown in Tab. 4, starting from MapTRv2 as our baseline, each module improves mAP. In addition, we also report the total unstable matching score u_t on the validation set, demonstrating that the prior position and structure of map elements improve the stability of matching.

Ablation study of decoder query prior. We compare various query priors under different BEV feature scales in Tab. 5. MAI in MGMap provides semantic priors for queries, but the improvement is limited. This limitation arises be-

Range	Method	AP _{div}	AP _{ped}	AP _{bou}	mAP
90×30m	MapTRv2	61.9	56.9	61.4	60.0
	PriorMapNet	66.5	62.0	66.1	64.9
60×60m	MapTRv2	61.5	58.8	61.0	60.5
	PriorMapNet	66.6	63.8	66.5	65.6
100×50m	MapTRv2	62.1	55.3	61.4	59.6
	SQD-MapNet	65.5	67.0	59.5	64.0
	PriorMapNet	67.4	62.5	65.0	65.0

Table 3: Quantitative evaluation on nuScenes dataset with enlarged BEV ranges. PriorMapNet maintains superiority.

PF	PPS	DMD	AP _{div}	AP _{ped}	AP _{bou}	mAP	u_t
-	-	-	60.5	60.5	61.8	60.9	0.413
✓	-	-	64.9	61.8	64.9	63.9	-
-	✓	-	64.6	62.8	65.8	64.4	0.365
✓	✓	-	68.7	63.6	68.0	66.8	-
✓	✓	✓	69.0	64.0	68.2	67.1	0.362

Table 4: Ablation study of our modules on nuScenes dataset. “PF”, “PPS” and “DMD” denote PF-Encoder, PPS-Decoder and DMD cross-attention, respectively. u_t is the total unstable matching score defined in Section 1.

cause semantic priors lack positional information crucial for vectorized map elements. We then integrate MAI with query position, but the mAP decreases as the semantic priors are not well-suited for query position. In contrast, our PPS provides prior position and structure, resulting in significant performance improvements. Compared with directly using clustering results as priors, abstracted priors perform better.

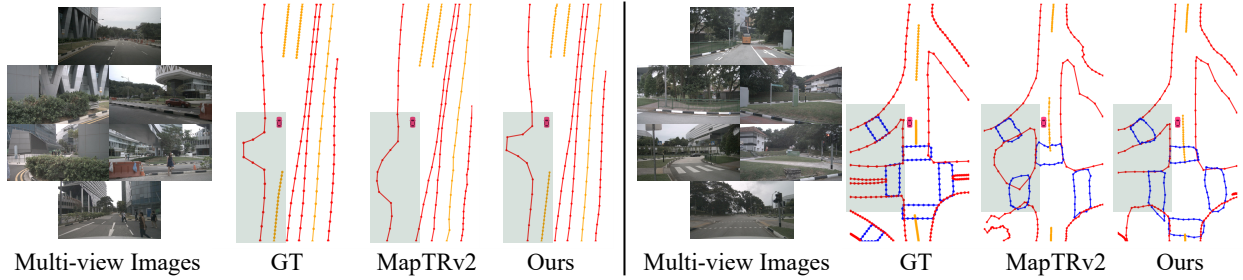


Figure 6: Qualitative results on nuScenes val set. We compare visualization results of PriorMapNet with MapTRv2 and corresponding GTs. Models are trained for 24 epochs. The green area indicates that our method achieves more accurate results.

F_{BEV}	Query Prior	AP_{div}	AP_{ped}	AP_{bou}	mAP
Single Scale	-	64.9	61.8	64.9	63.9
	MAI	65.0	62.7	64.8	64.2
	MAI-pos	58.3	51.0	62.3	57.2
	PPS-clst	64.6	63.8	66.9	65.1
	PPS	65.5	62.8	68.5	65.6
Multi Scales	-	67.5	61.7	65.8	65.0
	MAI	66.5	62.1	67.1	65.2
	MAI-pos	58.4	54.7	61.2	58.1
	PPS-clst	68.4	63.3	67.5	66.4
	PPS	68.7	63.6	68.0	66.8

Table 5: Ablation study of decoder query prior. “MAI” denotes Mask-Activated Instance in MGMap, and “MAI-pos” denotes integrating MAI with query position. “PPS-clst” denotes directly using clustering results as priors.

Ablation study of PF-Encoder design. We compare various BEV feature priors and encoders, as shown in Tab. 6. All GKT and BEVFormer methods utilize a single-layer architecture. To ensure a fair comparison, we incorporate auxiliary depth supervision across all experimental setups. LSS without prior is the encoder of MapTRv2. The third row denotes a two-layer BEVFormer encoder to exclude the impact of the number of encoder layers. The results show that LSS serves as a good prior generator. Results also demonstrate the effectiveness of Discriminative Loss.

Ablation study of DMD cross-attention design. We compare different decoupling designs of DMD cross-attention, including parallel and serial connection of two MSDA mechanisms, as shown in Tab. 7. In the serial connection, we compare different performance orders of MSDA along multi-sample and multi-scale dimensions. Experimental results demonstrate that our proposed DMD cross-attention improves efficiency and achieves superior performance.

5 Conclusion

In this paper, we introduce PriorMapNet to enhance online vectorized HD map construction with priors. To address the issue of unstable matching, we propose the PPS-Decoder, which provides reference points with position and structure priors clustered from the dataset. To embed BEV features

F_{BEV}	Prior	BEV Encoder	Dis. Loss	mAP
-	-	LSS-d	-	60.9
-	-	BEVFormer-d	-	57.3
BEVFormer-d	BEVFormer	-	-	59.6
GKT-d	BEVFormer	-	-	61.9
LSS-d	GKT	-	-	62.4
LSS-d	BEVFormer	-	-	63.3
LSS-d	BEVFormer	✓	-	63.9

Table 6: Ablation study of the PF-Encoder design. “Dis. Loss” denotes Discriminative Loss, and “-d” denotes auxiliary depth supervision of image features.

MSDA	AP_{div}	AP_{ped}	AP_{bou}	mAP	t_c (ms)
Vanilla	68.7	63.6	68.0	66.8	6.1
Parallel Connection	68.5	65.7	66.5	66.9	4.2
Sample-then-Scale	67.6	64.7	68.0	66.8	4.2
Scale-then-Sample	69.0	64.0	68.2	67.1	4.2

Table 7: Ablation study of the DMD cross-attention design. “Sample-then-Scale” denotes performing MSDA along multi-sample then multi-scale, and “Scale-then-Sample” denotes performing MSDA along reverse order. t_c denotes the inference time of cross-attention.

effectively, we propose the PF-Encoder which enhances the image-to-BEV transformation with BEV feature priors and leverages Discriminative Loss to improve the aggregation of map element embeddings. To reduce the computation complexity, we propose the DMD cross-attention, which performs cross-attention respectively along multi-scale and multi-sample. Our proposed PriorMapNet achieves state-of-the-art performance on nuScenes and Argoverse2 datasets.

Limitations and Future Work. Despite our development for online vectorized HD map construction, several limitations need to be addressed in future work. Firstly, our map element priors only incorporate positional information and lack semantic information, which limits the interaction and optimization of queries. Secondly, our method relies solely on single-frame sensor input, constraining the representation of temporally and spatially continuous map elements.

References

- Caesar, H.; Bankiti, V.; Lang, A. H.; Vora, S.; Liong, V. E.; Xu, Q.; Krishnan, A.; Pan, Y.; Baldan, G.; and Beijbom, O. 2020. nuscenes: A multimodal dataset for autonomous driving. In *Proceedings of the IEEE/CVF conference on computer vision and pattern recognition*, 11621–11631.
- Carion, N.; Massa, F.; Synnaeve, G.; Usunier, N.; Kirillov, A.; and Zagoruyko, S. 2020. End-to-end object detection with transformers. In *ECCV*, 213–229. Springer.
- Chen, S.; Cheng, T.; Wang, X.; Meng, W.; Zhang, Q.; and Liu, W. 2022. Efficient and robust 2d-to-bev representation learning via geometry-guided kernel transformer. *arXiv preprint arXiv:2206.04584*.
- He, K.; Zhang, X.; Ren, S.; and Sun, J. 2016. Deep residual learning for image recognition. In *Proceedings of the IEEE conference on computer vision and pattern recognition*, 770–778.
- Hu, Y.; Yang, J.; Chen, L.; Li, K.; Sima, C.; Zhu, X.; Chai, S.; Du, S.; Lin, T.; Wang, W.; et al. 2023. Planning-oriented autonomous driving. In *Proceedings of the IEEE/CVF Conference on Computer Vision and Pattern Recognition*, 17853–17862.
- Huang, J.; Huang, G.; Zhu, Z.; Ye, Y.; and Du, D. 2021. Bevdet: High-performance multi-camera 3d object detection in bird-eye-view. *arXiv preprint arXiv:2112.11790*.
- Jiang, Z.; Zhu, Z.; Li, P.; Gao, H.-a.; Yuan, T.; Shi, Y.; Zhao, H.; and Zhao, H. 2024. P-MapNet: Far-seeing map generator enhanced by both SDMap and HDMap priors. *arXiv preprint arXiv:2403.10521*.
- Lang, A. H.; Vora, S.; Caesar, H.; Zhou, L.; Yang, J.; and Beijbom, O. 2019. Pointpillars: Fast encoders for object detection from point clouds. In *Proceedings of the IEEE/CVF Conference on Computer Vision and Pattern Recognition*, 12697–12705.
- Li, F.; Zhang, H.; Liu, S.; Guo, J.; Ni, L. M.; and Zhang, L. 2022a. Dn-detr: Accelerate detr training by introducing query denoising. In *Proceedings of the IEEE/CVF Conference on Computer Vision and Pattern Recognition*, 13619–13627.
- Li, H.; Huang, Z.; Wang, Z.; Rong, W.; Wang, N.; and Liu, S. 2024a. Enhancing 3D Lane Detection and Topology Reasoning with 2D Lane Priors. *arXiv preprint arXiv:2406.03105*.
- Li, Q.; Wang, Y.; Wang, Y.; and Zhao, H. 2022b. Hdmapnet: An online hd map construction and evaluation framework. In *ICRA*, 4628–4634. IEEE.
- Li, S.; Yang, K.; Shi, H.; Zhang, J.; Lin, J.; Teng, Z.; and Li, Z. 2023a. Bi-Mapper: Holistic BEV Semantic Mapping for Autonomous Driving. *IEEE Robotics and Automation Letters*.
- Li, T.; Jia, P.; Wang, B.; Chen, L.; JIANG, K.; Yan, J.; and Li, H. 2024b. LaneSegNet: Map Learning with Lane Segment Perception for Autonomous Driving. In *The Twelfth International Conference on Learning Representations*.
- Li, Y.; Bao, H.; Ge, Z.; Yang, J.; Sun, J.; and Li, Z. 2022c. Bevstereo: Enhancing depth estimation in multi-view 3d object detection with dynamic temporal stereo. *arXiv preprint arXiv:2209.10248*.
- Li, Y.; Ge, Z.; Yu, G.; Yang, J.; Wang, Z.; Shi, Y.; Sun, J.; and Li, Z. 2023b. Bevdepth: Acquisition of reliable depth for multi-view 3d object detection. In *Proceedings of the AAAI Conference on Artificial Intelligence*, volume 37, 1477–1485.
- Li, Z.; Wang, W.; Li, H.; Xie, E.; Sima, C.; Lu, T.; Qiao, Y.; and Dai, J. 2022d. Bevformer: Learning bird’s-eye-view representation from multi-camera images via spatiotemporal transformers. In *European conference on computer vision*, 1–18. Springer.
- Liang, M.; Yang, B.; Hu, R.; Chen, Y.; Liao, R.; Feng, S.; and Urtasun, R. 2020. Learning lane graph representations for motion forecasting. In *Computer Vision—ECCV 2020: 16th European Conference, Glasgow, UK, August 23–28, 2020, Proceedings, Part II 16*, 541–556. Springer.
- Liao, B.; Chen, S.; Wang, X.; Cheng, T.; Zhang, Q.; Liu, W.; and Huang, C. 2022. MapTR: Structured Modeling and Learning for Online Vectorized HD Map Construction. In *ICLR*.
- Liao, B.; Chen, S.; Zhang, Y.; Jiang, B.; Zhang, Q.; Liu, W.; Huang, C.; and Wang, X. 2023. Maptrv2: An end-to-end framework for online vectorized hd map construction. *arXiv preprint arXiv:2308.05736*.
- Lin, T.-Y.; Dollár, P.; Girshick, R.; He, K.; Hariharan, B.; and Belongie, S. 2017. Feature pyramid networks for object detection. In *Proceedings of the IEEE conference on computer vision and pattern recognition*, 2117–2125.
- Liu, S.; Li, F.; Zhang, H.; Yang, X.; Qi, X.; Su, H.; Zhu, J.; and Zhang, L. 2022a. DAB-DETR: Dynamic Anchor Boxes are Better Queries for DETR. In *International Conference on Learning Representations*.
- Liu, S.; Ren, T.; Chen, J.; Zeng, Z.; Zhang, H.; Li, F.; Li, H.; Huang, J.; Su, H.; Zhu, J.; et al. 2023a. Detection transformer with stable matching. In *Proceedings of the IEEE/CVF International Conference on Computer Vision*, 6491–6500.
- Liu, X.; Wang, S.; Li, W.; Yang, R.; Chen, J.; and Zhu, J. 2024a. Mgmmap: Mask-guided learning for online vectorized hd map construction. In *Proceedings of the IEEE/CVF Conference on Computer Vision and Pattern Recognition*, 14812–14821.
- Liu, Y.; Yan, J.; Jia, F.; Li, S.; Gao, Q.; Wang, T.; Zhang, X.; and Sun, J. 2022b. Petrv2: A unified framework for 3d perception from multi-camera images. *arXiv preprint arXiv:2206.01256*.
- Liu, Y.; Yuan, T.; Wang, Y.; Wang, Y.; and Zhao, H. 2023b. Vectormapnet: End-to-end vectorized hd map learning. In *ICML*, 22352–22369. PMLR.
- Liu, Z.; Zhang, X.; Liu, G.; Zhao, J.; and Xu, N. 2024b. Leveraging Enhanced Queries of Point Sets for Vectorized Map Construction. In *European Conference on Computer Vision*.

- Loshchilov, I.; and Hutter, F. 2016. Sgdr: Stochastic gradient descent with warm restarts. *arXiv preprint arXiv:1608.03983*.
- Loshchilov, I.; and Hutter, F. 2017. Decoupled weight decay regularization. *arXiv preprint arXiv:1711.05101*.
- Luo, K. Z.; Weng, X.; Wang, Y.; Wu, S.; Li, J.; Weinberger, K. Q.; Wang, Y.; and Pavone, M. 2023. Augmenting Lane Perception and Topology Understanding with Standard Definition Navigation Maps. *arXiv preprint arXiv:2311.04079*.
- Meng, D.; Chen, X.; Fan, Z.; Zeng, G.; Li, H.; Yuan, Y.; Sun, L.; and Wang, J. 2021. Conditional detr for fast training convergence. In *Proceedings of the IEEE/CVF international conference on computer vision*, 3651–3660.
- Neven, D.; De Brabandere, B.; Georgoulis, S.; Proesmans, M.; and Van Gool, L. 2018. Towards end-to-end lane detection: an instance segmentation approach. In *2018 IEEE intelligent vehicles symposium (IV)*, 286–291. IEEE.
- Peng, L.; Chen, Z.; Fu, Z.; Liang, P.; and Cheng, E. 2023. BEVSegFormer: Bird’s Eye View Semantic Segmentation From Arbitrary Camera Rigs. In *WACV*, 5935–5943.
- Phillion, J.; and Fidler, S. 2020. Lift, splat, shoot: Encoding images from arbitrary camera rigs by implicitly unprojecting to 3d. In *Computer Vision—ECCV 2020: 16th European Conference, Glasgow, UK, August 23–28, 2020, Proceedings, Part XIV 16*, 194–210. Springer.
- Tan, M.; and Le, Q. 2019. Efficientnet: Rethinking model scaling for convolutional neural networks. In *International conference on machine learning*, 6105–6114. PMLR.
- Vaswani, A.; Shazeer, N.; Parmar, N.; Uszkoreit, J.; Jones, L.; Gomez, A. N.; Kaiser, Ł.; and Polosukhin, I. 2017. Attention is all you need. *Advances in neural information processing systems*, 30.
- Wang, S.; Jia, F.; Liu, Y.; Zhao, Y.; Chen, Z.; Wang, T.; Zhang, C.; Zhang, X.; and Zhao, F. 2024. Stream query denoising for vectorized hd map construction. *arXiv preprint arXiv:2401.09112*.
- Wang, Y.; Guizilini, V. C.; Zhang, T.; Wang, Y.; Zhao, H.; and Solomon, J. 2022. Detr3d: 3d object detection from multi-view images via 3d-to-2d queries. In *Conference on Robot Learning*, 180–191. PMLR.
- Wilson, B.; Qi, W.; Agarwal, T.; Lambert, J.; Singh, J.; Khandelwal, S.; Pan, B.; Kumar, R.; Hartnett, A.; Pontes, J. K.; et al. 2023. Argoverse 2: Next generation datasets for self-driving perception and forecasting. *arXiv preprint arXiv:2301.00493*.
- Xu, Z.; Wong, K.-Y. K.; and Zhao, H. 2023. InsMapper: Exploring Inner-instance Information for Vectorized HD Mapping. *arXiv preprint arXiv:2308.08543*.
- Yan, Y.; Mao, Y.; and Li, B. 2018. Second: Sparsely embedded convolutional detection. *Sensors*, 18(10): 3337.
- Yang, C.; Chen, Y.; Tian, H.; Tao, C.; Zhu, X.; Zhang, Z.; Huang, G.; Li, H.; Qiao, Y.; Lu, L.; et al. 2023. BEVFormer v2: Adapting Modern Image Backbones to Bird’s-Eye-View Recognition via Perspective Supervision. In *Proceedings of the IEEE/CVF Conference on Computer Vision and Pattern Recognition*, 17830–17839.
- Zhou, Y.; Zhang, H.; Yu, J.; Yang, Y.; Jung, S.; Park, S.-I.; and Yoo, B. 2024. HlMap: Hybrid Representation Learning for End-to-end Vectorized HD Map Construction. In *Proceedings of the IEEE/CVF Conference on Computer Vision and Pattern Recognition*, 15396–15406.
- Zhou, Z.; Ye, L.; Wang, J.; Wu, K.; and Lu, K. 2022. Hivt: Hierarchical vector transformer for multi-agent motion prediction. In *Proceedings of the IEEE/CVF Conference on Computer Vision and Pattern Recognition*, 8823–8833.
- Zhu, X.; Su, W.; Lu, L.; Li, B.; Wang, X.; and Dai, J. 2020. Deformable detr: Deformable transformers for end-to-end object detection. *arXiv preprint arXiv:2010.04159*.

Supplementary Material

In the supplementary material, we provide more details, experiments, and analysis of the proposed PriorMapNet, including:

- More implementation details of our method;
- Additional ablation studies on hyperparameters;
- Difference with previous SOTA methods;
- More qualitative results and failure cases.

S1 More Implementation Details

Feature extraction and multi-modality fusion. Multi-modality inputs consist of multi-view cameras and LiDAR data. For backbones, we utilize ResNet50 (He et al. 2016) for image features extraction and SECOND (Yan, Mao, and Li 2018) for point cloud features extraction. The input image size is 480×800 . The voxel size for point cloud is set to $[0.1\text{m}, 0.1\text{m}, 0.2\text{m}]$, and the LiDAR BEV features are up-sampled to align with camera BEV features. For BEV feature fusion, we concatenate camera and LiDAR BEV features along feature channels and use a convolution layer to fuse them.

Encoder and decoder. Following MapTRv2 (Liao et al. 2023), we add an auxiliary depth loss for LSS to generate BEV query priors effectively. The PPS-Decoder contains 6 layers to refine the outputs iteratively. In addition to 50 instance-level queries, there are another 300 one-to-many queries that are used to speed up convergence during training. Priors are not used for one-to-many queries.

Training. We use the AdamW optimizer (Loshchilov and Hutter 2017) with an initial learning rate of 6×10^{-4} , and apply the Cosine Annealing learning rate scheduler with a linear warm-up phase (Loshchilov and Hutter 2016). Except for our Discriminative Loss, other training and loss settings keep in line with our baseline MapTRv2.

S2 Additional Ablation Studies

Ablation study on the number of prior queries. We cluster 50 map elements and abstract the position information of the first N_{pri} elements, as shown in Fig. 2. To most effectively utilize the prior position and structure, we compare the results of different numbers of prior queries (*i.e.* N_{pri}), as shown in Tab. S1. Utilizing 9 prior queries achieves the best performance. Too few prior queries cannot fully utilize the prior, while too many prior queries limit the learning ability of learnable queries.

Ablation study on the loss weights. The Discriminative Loss is defined as $L_{\text{dis}} = \lambda_1 L_{\text{var}} + \lambda_2 L_{\text{dist}}$. Following LaneNet (Neven et al. 2018), we set $\lambda_1 = \lambda_2 = \lambda$. In order to obtain the most effective auxiliary discriminative supervision, we compare the results under different loss weights (*i.e.* λ), as shown in Tab. S2. Experimental results show the effectiveness of Discriminative Loss, and the best performance can be achieved when $\lambda = 1$.

Ablation study on the borders of the variance and distance loss. δ_v and δ_d are respectively the borders of the

N_{pri}	AP_{div}	AP_{ped}	AP_{bou}	mAP
0	67.5	61.7	65.8	65.0
5	67.2	62.7	67.8	65.9
9	68.7	63.6	68.0	66.8
10	67.3	63.8	68.8	66.7
20	68.1	63.5	68.0	66.5
50	68.4	63.3	67.5	66.4

Table S1: Ablation study of the number of prior queries. Utilizing 9 prior queries achieves the best performance.

λ	AP_{div}	AP_{ped}	AP_{bou}	mAP
0	64.3	60.9	64.8	63.3
0.5	65.6	61.6	63.7	63.6
1	64.9	61.8	64.9	63.9
2	65.1	60.7	64.6	63.5
3	64.5	60.1	65.0	63.2

Table S2: Ablation study of the weight of Discriminative Loss. We set $\lambda_1 = \lambda_2 = \lambda$ and setting $\lambda = 1$ achieves the best performance.

δ_d	AP_{div}	AP_{ped}	AP_{bou}	mAP
1	64.8	60.5	64.2	63.2
3	64.9	61.8	64.9	63.9
6	66.0	61.2	63.9	63.7
12	65.4	61.0	64.5	63.6

Table S3: Ablation study of the borders of the variance and distance loss. We set $\delta_d = 6\delta_v$ and setting $\delta_d = 3$ achieves the best performance.

variance and distance loss. Following LaneNet (Neven et al. 2018), we set $\delta_d = 6\delta_v$. To embed the BEV features effectively, we compare the results under different borders of the distance loss (*i.e.* δ_d), as shown in Tab. S3. Experiments are conducted under $\lambda = 1$. Experimental results show that the best performance can be achieved when $\delta_d = 3$.

S3 Difference with Previous SOTA Methods

We highlight the key distinctions between our PriorMapNet and previous SOTA methods, including MapTRv2 (Liao et al. 2023), MGMap (Liu et al. 2024a), HIMap (Zhou et al. 2024), MapQR (Liu et al. 2024b) and InsMapper (Xu, Wong, and Zhao 2023). We compare the decoders in Fig. S1, which are the core of these methods.

Motivation and model design. Our motivation and model design diverge from those of previous SOTA methods. PriorMapNet starts from the issue of *unstable matching* and utilizes pre-computed clustered priors to initialize reference points. Fitted from the map elements in the dataset, prior ref-

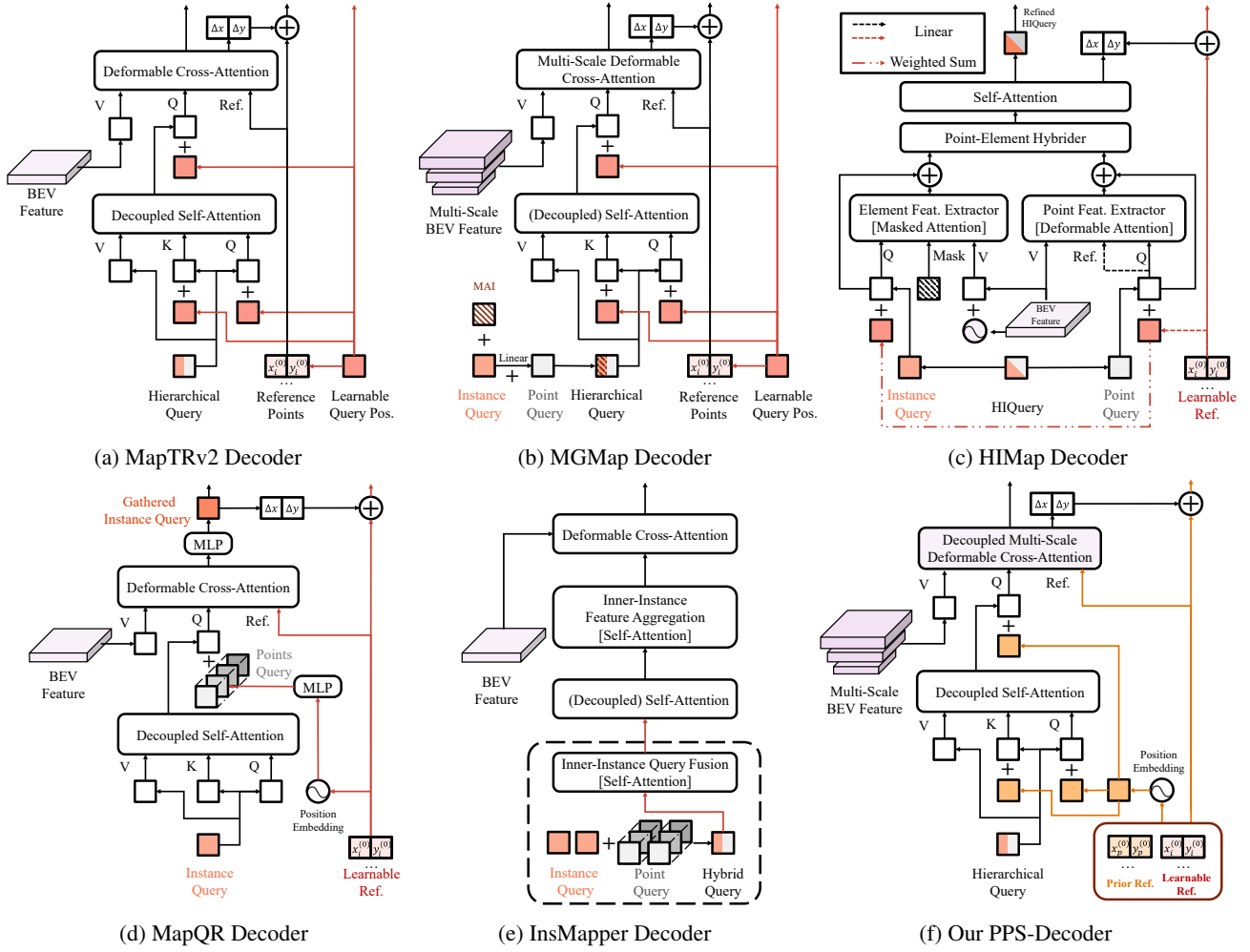


Figure S1: Comparison of the decoders of previous SOTA methods: (a) MapTRv2, (b) MGMap, (c) HIMap, (d) MapQR, (e) InsMapper and (f) our proposed PriorMapNet. (a), (b) and (d) are based on their open-source code, and (c) is based on the implementation details and equations from the paper. For simplicity, we only show the first layer in the transformer decoder. Since InsMapper currently has no open-source code and the specific implementation process is not detailed in the paper, we only show the general structure of its decoder. To highlight the key distinctions between our PriorMapNet and previous SOTA methods, we mark the randomly initialized learnable query position embeddings and reference points in light red, and mark our prior-aware query position embeddings and reference points in yellow.

reference points lower the learning difficulty and achieve stable matching. In contrast, HIMap, MapQR, and InsMapper ignore query priors and use randomly initialized reference points. Based on MapTR series methods, they explore the correlations between instances and points, which introduce additional modules and computational complexity. MGMap proposes Mask-Activated Instance to learn map instance segmentation results and provides semantic priors for instance queries. However, semantic priors lack positional information, which is essential for vectorized map elements. Our PPS-Decoder provides prior position and structure, resulting in significant performance improvements.

Performance. Our PriorMapNet surpasses previous SOTA methods on nuScenes and Argoverse 2 dataset, as illustrated in Tab. 1 and Tab. 2. PriorMapNet achieves SOTA perfor-

mance under different modalities on nuScenes dataset and different dimensions on Argoverse 2 dataset, demonstrating the generalizability of our method.

S4 Qualitative Results and Failure Cases

We show more qualitative results and failure cases on nuScenes val set in Fig. S2 and Fig. S3, respectively. For each example, the first column represents multi-view camera images. The second column shows the prediction GT. The third and fourth columns respectively show the predicted results of MapTRv2 and our PriorMapNet. Visualization results illustrate that PriorMapNet achieves improved results than MapTRv2. However, in some complex scenes such as intersections, our method fails to predict some map elements, showing our limitations and requiring future work.

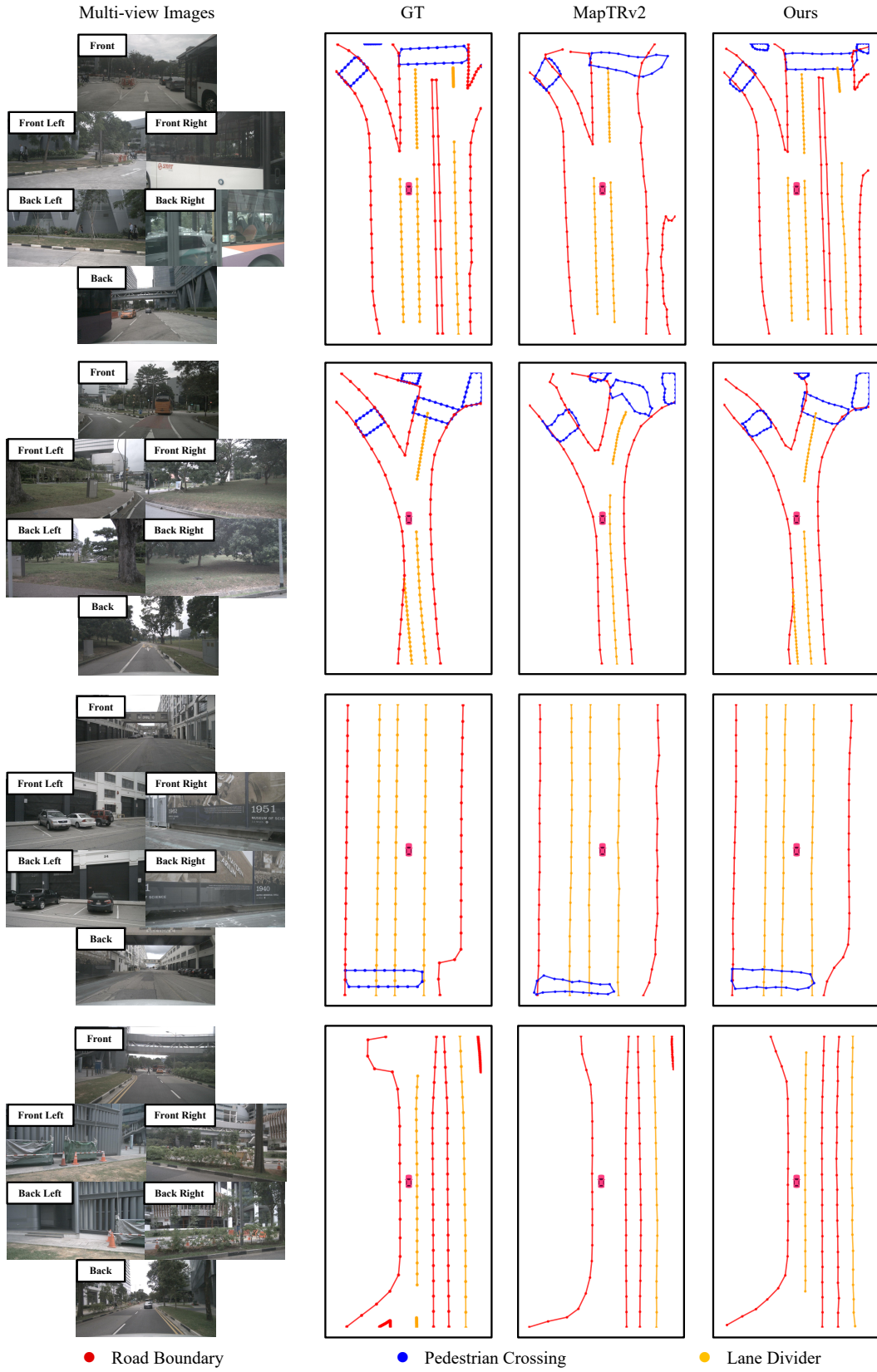


Figure S2: Visualization of MapTRv2 and PriorMapNet results and the corresponding GTs. Models are trained for 24 epochs.

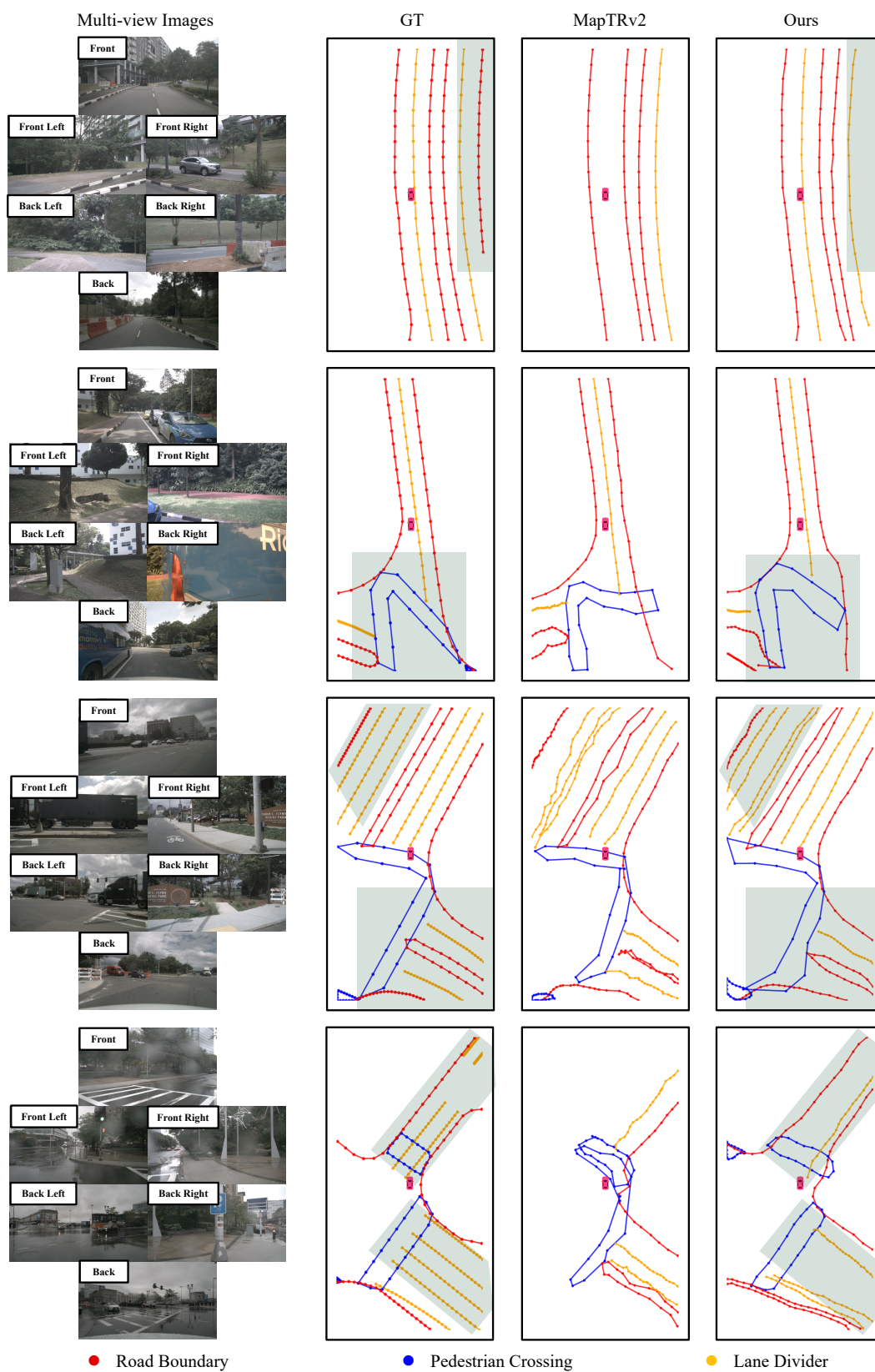


Figure S3: Visualization of failure cases. The green areas indicate locations where our method fails to predict accurate results.